Collaborative membrane activity and receptor-dependent tumor cell targeting for precise nanoparticle delivery in CXCR4+ colorectal cancer

Rita Sala [1, 2 ¥], Laura Sánchez-García [1, 3, 4 ¥], Naroa Serna [1, 3, 4], María Virtudes Céspedes [1,2], Isolda Casanova [1,2], Mònica Roldán [5,6], Alejandro Sánchez-Chardi [7], Ugutz Unzueta [1,2], Esther Vázquez [1, 3, 4 *], Ramón Mangues [1,2 *], Antonio Villaverde [1, 3, 4 *]

[1] CIBER de Bioingeniería, Biomateriales y Nanomedicina (CIBER-BBN), C/ Monforte de Lemos 3-5, 28029 Madrid, Spain

[2] Institut d'Investigacions Biomèdiques Sant Pau and Josep Carreras Research Institute, Hospital de la Santa Creu i Sant Pau, 08041 Barcelona, Spain

[3] Institut de Biotecnologia i de Biomedicina, Universitat Autònoma de Barcelona, Bellaterra, 08193 Barcelona, Spain

[4] Departament de Genètica i de Microbiologia, Universitat Autònoma de Barcelona, Bellaterra, 08193 Barcelona, Spain

[5] Unitat de Microscòpia Confocal. Servei d'Anatomia Patològica, Institut Pediàtric de Malalties Rares (IPER), Hospital Sant Joan de Déu, Esplugues de Llobregat, Barcelona, Spain

[6] Institut de Recerca Sant Joan de Déu, Esplugues de Llobregat, Barcelona, Spain.

[7] Departament de Biologia Evolutiva, Ecologia i Ciències Ambientals, Facultat de Biologia, Universitat de Barcelona, 08028 Barcelona, Spain

* Corresponding authors
¥ Equally contributed

Keywords: protein materials, self-assembling, fusogenic peptide, colorectal cancer; CXCR4; active targeting

Abstract

By the appropriate selection of functional peptides and proper accommodation sites, we have generated a set of multifunctional proteins that combine selectivity for CXCR4+ cell binding and relevant endosomal escape capabilities linked to the viral peptide HA2. In particular, the construct T22-GFP-HA2-H6 forms nanoparticles that upon administration in mouse models of human, CXCR4+ colorectal cancer, accumulates in primary tumor at levels significantly higher than the parental T22-GFP-H6 HA2-lacking version. The *in vivo* application of a CXCR4 antagonist has confirmed the prevalence of the CXCR4+ tumor tissue selectivity over unspecific cell penetration, upon systemic administration of the material. Such specificity is combined with improved endosomal escape, what overall results in a precise and highly efficient tumor biodistribution. These data strongly support the functional recruitment as a convenient approach to generate protein materials for clinical applications. More precisely, they also support the unexpected concept that enhancing the unspecific membrane activity of a protein material does not necessarily compromise, but it can even improve, the selective cell targeting offered by an accompanying functional module.

1. Introduction

The plasticity of proteins as highly versatile macromolecules allows functional recruitment by simple genetic fusion, upon selection of appropriate protein domains [1]. This approach permits the combination, in modular polypeptides constructed *de novo*, of diverse functionalities such as self-assembling and specific interaction with cells or cell components, what results in functional materials usable in different biomedical applications [2-10]. Among other uses, regular nanoscale oligomers are promising carriers for cell-targeted drug delivery [11-13], a popular aim when administering cytotoxic drugs in cancer therapies [14-18]. Protein nanoparticles, because of the above mentioned versatility, can be easily functionalized with peptidic ligands of cell surface markers for active targeting and subsequent endosome-mediated cell internalization. On the other hand, endosomal escape, required for drug delivery, is a major bottleneck when using protein-based drug vehicles [19, 20], that are sensitive to proteolysis in endocytic compartments. Therefore, under the functional recruitment concept, it would be extremely useful to combine precise cell targeting (through specific ligands of cell surface markers) and endosomal escape (through membrane-active peptides, that unfortunately, lack cell specificity) in single nanoparticles. However, how receptor-specific and receptor-unspecific cell contacts, empowered by a ligand and a fusogenic peptide respectively, would combine in drug vehicles, is a neglected issue. In this context, we have previously functionalized self-assembling protein nanoparticles (mostly based on GFP) [21] with the peptide T22, targeted to the highly relevant, cancer stem cell marker of CXCR4 [22, 23]. These nanoparticles are formed by ten individual T22-GFP-H6 building blocks [21] that keep their native GFP conformation [24], and that are stably connected by divalent cations coordinated with the carboxy-terminal histidine tails [25]. When conjugated with conventional antitumoral drugs, T22-GFP-H6

3

nanoparticles promote successful unusually high tumor tissue drug accumulation and highly selective destruction of metastatic foci in animal models of colorectal cancer [26]. To improve drug and vehicle stability during intracellular delivery, we have favoured the endosomal escape of the construct by the incorporation of either the fusogenic HA2 peptide from the influenza virus hemagglutinin [27-29] or the synthetic pore-forming peptide GW-H1 [30, 31], into T22-GFP-H6 building blocks, to effectively trigger an early escape from endosomes [32]. The resulting modular nanoparticles dramatically gained cell penetrability and endosomal escape in cell culture but at expenses of CXCR4 selectivity, that was importantly reduced [33, 34]. Despite this preliminary result, how such simultaneous gain of penetrability and loss of cell specificity promoted by endosomolytic peptides would affect *in vivo* biodistribution and tumor accumulation of the nanoparticle remained to be assessed.

2. Materials and methods

2.1. Protein production and purification

Modular proteins T22-HA2-GFP-H6 and T22-GFP-HA2-H6 (Figure 1A) were produced in

Escherichia coli Origami B strain (BL21, OmpT⁻, Lon⁻, TrxB⁻, Gor⁻; Novagen). Protein

production was induced at an OD550 of ~ 0.5 - 0.7 by the addition of 0.1 mM and 0.01 mM

of isopropyl-β-thiogalactopyronaside (IPTG), respectively. After overnight production at

16 °C (T22-HA2-GFP-H6) and 20 °C (T22-GFP-HA2-H6) cells were harvested by centrifugation

(5,000 g, 15 min, 4 ºC) and stored at -80 ºC until use. Bacterial pellets were resuspended in

Wash buffer (20 mM Tris pH 8.0, 500 mM NaCl and 10 mM imidazole) in presence of a

protease inhibitor cocktail (Complete EDTA-Free, Roche) for purification purposes. Then,

bacterial cells were disrupted by French Press at 1,200 psi for 3 rounds (Thermo FA-078A)

and centrifuged (15,000 g, 45 min, 4 ºC) to separate the soluble from the insoluble fraction.

After 0.22 µm filtration, proteins were purified by Immobilized Metal Affinity

Chromatography (IMAC) using a HiTrap Chelating HP column (GE Healthcare) in an ÄKTA

pure system (GE Healthcare). Proteins were eluted by a one-step of Elution buffer (20 mM

Tris pH 8.0, 500 mM NaCl and 500 mM imidazole) and further dialyzed against 166 mM

NaCO₃H (T22-HA2-GFP-H6) and 166 mM NaCO₃H 333 mM NaCl buffers (T22-GFP-HA2-H6).

2.2 Physicochemical characterization

Protein integrity and purity was assessed by Sodium Dodecyl Sulphate Polyacrylamide Gel

Electrophoresis (SDS-PAGE) and Western blotting using an anti-His monoclonal antibody

(Santa Cruz Biotechnology). The molecular mass of T22-HA2-GFP-H6 and T22-GFP-HA2-H6

proteins was determined by Matrix-Assisted Laser Desorption Ionization Time-of-Flight

(MALDI-TOF) mass spectrometry, while the volume size distribution was determined by

Dynamic Light Scattering (DLS) at 633 nm in a Zetasizer Nano ZS (Malvern Instruments Limited). Additionally, fluorescence of the GFP-based nanoparticles was determined by a Varian Cary Eclipse Fluorescence Spectrophotometer (Agilent Technologies), through an excitation wavelength at 450 nm and detection at 510 nm. Protein stability, was assessed in human sera (Sigma-Aldrich) at 37 ºC for 0, 2, 5 and 24 h. Then, protein integrity was evaluated by Western blot using an anti-His monoclonal antibody (Santa Cruz Biotechnology) for the specific immunodetection of the His-tag. Additionally, Precision Plus Protein All Blue Standards (BioRad) was used to confirm the expected molecular weight of the samples.

2.3 Cell culture and flow cytometry

$CXCR4^+$ HeLa cells were maintained in MEM Alpha (Minimum Essential Medium α, Gibco) supplemented with 10 % foetal bovine serum (Gibco) at 37 °C and 5 % CO_2 in a humidified atmosphere. In order to assess *in vitro* the CXCR4 specificity of HA2-bearing proteins, HeLa cells were scattered (30,000 cells/well) in 24-well plates and incubated during 24 h at 37 ºC until reaching 70 % confluence. Then, the antagonist AMD3100, which is expected to inhibit the interaction between T22 and CXCR4 receptor, was added at 1:10 ratio 1 h prior to protein incubation. Finally, T22-HA2-GFP-H6 and T22-GFP-HA2-H6 were incubated for 1 h at a final concentration of 0.1 μM. The obtained samples (performed in duplicate) were analysed by a FACS-Canto system (Becton Dickinson) using a 15 mW air-cooled argon ion laser at 488 nm excitation.

2.4 Confocal laser scanning microscopy

For confocal studies of nanoparticle uptake by cells, HeLa cell line was cultured on Mat-Teck culture dishes (Mat Tek Corp.). Protein nanoparticles were added at 0.5 μM, and after 24 h

of exposure, nuclei were labelled with 5 μg/ml Hoechst 33342 (Molecular Probes) and plasma membranes with 2.5 μg/ml CellMaskTM Deep Red (Molecular Probes), for 5 min in absence of light. Live cells were washed in PBS (Sigma-Aldrich) and recorded with a TCS-SP5 confocal laser scanning microscope (Leica Microsystems) using a Plan Apo 63x / 1.4 (oil HC x PL APO lambda blue) objective. Hoechst 33342 was excited with a blue diode (405 nm) and detected within a 415-460 nm range. Proteins were excited by the 488 nm argon laser line and detected within a 525-545 nm range. CellMask was excited with a HeNe laser (633 nm) and within a 650-775 nm range. To determine precise intracellular localization, stacks of 20 to 30 sections were collected every 0.5 μm along the cell thickness. The obtained projections of the series were generated with Leica LAS X software, and three-dimensional models were produced using Imaris v. 7.2.1 software (Bitplane).

2.5 Ultrastructural characterization

The ultrastructure of the nanoparticles was evaluated with a high resolution electron microscope at a nearly native state. Drops of 3 μl of each nanoparticle samples (T22-GFP-H6, T22-HA2-GFP-H6 and T22-GFP-HA2-H6) at a concentration of 0.25 μg/μl were directly deposited on conductive silicon wafers (Ted Pella Inc.) for 1 min, cleared few seconds in deionized water, air dried, and immediately observed without coating in a FESEM Merlin (Zeiss) operating at 1 kV and equipped with a high resolution in-lens secondary electron detector.

2.6 *In vivo* biodistribution studies

All *in vivo* experiments were approved by the institutional animal Ethics Committee of Hospital Sant Pau. Five-week-old female Swiss nu/nu mice weighing between 18 and 20 g

(Charles River) and maintained in specific-pathogen-free (SPF) conditions, were used for the *in vivo* biodistribution studies. We used a subcutaneous colorectal cancer mouse model derived from the patient sample M5. To generate this model, 10 mg of M5 tumor tissue obtained from a donor animal were implanted in the subcutis of Swiss nu/nu. When tumors reached a volume of approximately 500 mm^3 we performed biodistribution assays of both T22-HA2-GFP-H6 and T22-GFP-HA2-H6 nanoparticles at three different times, namely 2, 5 and 24 h. We used as a control of biodistribution the T22-GFP-H6 nanoparticle. Each group of mice (n=2) received 200 µg single i.v. bolus of one of these three nanoparticles. Control animals (n=2) were i.v. administered with 150 µl of buffer. At 2, 5 and 24 hours after the i.v. injection, mice were euthanized and subcutaneous tumors and normal organs, including brain, lung and heart, kidney, liver, and bone marrow were collected. Biodistribution of fluorescent nanoparticles was determined measuring *ex vivo* the fluorescence emitted by tumors and normal organs using the IVIS Spectrum equipment (PerkinElmer Inc). The fluorescent signal (FLI) was first digitalized, displayed as a pseudocolor overlay, and expressed as radiant efficiency. FLI values were calculated subtracting the FLI signal from the protein-treated mice by the FLI auto-fluorescent signal of control mice.

2.7 *In vivo* competition assays

The selectivity of the T22-GFP-HA2-H6 nanoparticle for CXCR4$^+$ tissues was analyzed in the same M5 subcutaneous CRC mouse model. For competition studies we used the CXCR4 antagonist AMD3100 (Sigma-Aldrich) and T22-GFP-H6 as a control of selectivity. Mice were randomized in 5 groups (n=2). The T22-GFP-H6 and T22-GFP-HA2-H6 groups received a 200 µg i.v. bolus of the corresponding protein. The AMD3100 competition groups were subcutaneously administered with three doses of 10 mg/kg of AMD3100 (1 h before, and 1

and 2 h after the nanoparticles injection). The control group received a i.v. bolus of buffer.

Mice were euthanized 5 h after nanoparticles injection and the GFP fluorescence emitted by

tumors and non-target organs was determined.

2.8 Histopathology and toxicity in normal organs

Sections of paraffin-embedded samples of non-target organs (brain, lung and heart, kidney,

liver, and bone marrow) were hematoxylin and eosin (H&E) stained and the presence of

toxicity was analyzed using an Olympus BX51 microscope (Olympus). Images were acquired

using an Olympus DP72 digital camera (Olympus).

2.9. Statistical analysis

The data of the *in vivo* experiments were reported as mean ± SE. AUC analysis was measured

using the GraphPad Prism v6 software and expressed as relative units. Results were analysed

using the Student's t-test, considering statistically significant the observed differences at a

probability $p<0.05$. Statistical calculations were performed using SPSS software v21.

3. Results and discussion

Upon systemic injection in mouse models of CXCR4^{+} human cancers, protein nanoparticles formed by T22-GFP-H6 and other derived self-assembling proteins are stable in blood and accumulate, intracellularly, in tumoral tissues, with poor or not detectable presence in non-target tissues [21, 35]. They show a first half-life of around 20 min to biodistribute in the blood compartment, followed by a longer elimination phase that yielded a high recirculation time of around 1 day [36, 37]. T22-GFP-H6 was used as a scaffold to accommodate the fusogenic peptide HA2 [27-29] (in alternative insertion sites) and to test then the combination of this membrane-active peptide, that acts in a receptor-independent way, and T22, a specific ligand of the tumoral marker CXCR4 [38]. To discriminate between potential exclusive or cooperative effects of HA2 and T22, we planned to study the biodistribution of T22-HA2-GFP-H6 and T22-GFP-HA2-H6 (Figure 1 A), in a mouse model of CXCR4^{+} human colorectal cancer. Previous to that, we determined that these proteins assembled as stable nanoparticles of 30 and 45 nm respectively (Figure 1 B), that while being all fluorescent, showed differential emission values (Figure 1 A, bottom). In addition, they were stable in serum upon prolonged *in vitro* incubation (Figure 1 C) and efficiently penetrate cultured CXCR4^{+} HeLa cells, being nicely traceable by their fluorescence (Figure 1 D). However, these proteins exhibited differential degrees of CXCR4-dependent cell penetration in cell culture (Figure 1 A, [33]), being the highest in the case of T22-GFP-H6 and negligible in the case of T22-HA2-GFP-H6. This indicated that HA2 reduced, at least in vitro, the CXCR4-specificity in cell penetration regarding the parental T22-GFP-H6. Samples to be administered to animals were also fluorescent enough for *in vivo* tracking (Figure 1 E), with degree of emission in agreement with the specific fluorescence of the protein materials (Figure 1 A, bottom).

In a next step, we administered intravenously T22-HA2-GFP-H6 and T22-GFP-HA2-H6, and the parental T22-GFP-H6 protein acting as control (Figure 1 A), in mice bearing M5 subcutaneous colorectal cancer (CRC) tumors with high expression of CXCR4 [39]. At different times upon single dose injections, T22-GFP-H6 accumulated in subcutaneous tumors at levels comparable to those previously described in similar animal models [21]. Interestingly, T22-HA2-GFP-H6 nanoparticles rendered a numerically similar result (Figure 2 A, B). However, a fast and efficient tumor retention of T22-GFP-HA2-H6 was unexpectedly observed, peaking between 2 and 5 h (Figure 2 C), that was necessarily linked to the accommodation of the viral HA2 peptide at the particular site between GFP and H6 modules (Figure 1 A). None of these proteins were observed at significant levels in non-target organs, at exception of some background of T22-GFP-HA2-H6 in the liver (Figure 3 A, B). However, the histopathology of liver and kidney in T22-GFP-HA2-H6-treated animals revealed a complete absence of lesions, indicative of no side toxicity (Figure 3 C) and supporting the biological safety of the protein.

In cell culture, T22-GFP-HA2-H6 showed a very efficient CXCR4$^+$ cell penetrability, around three-fold over the parental T22-GFP-H6 (specially at low protein doses) (Figure 1D, [33]), what is in nice agreement with the data obtained in animal models (Figure 2). However, in our defined experimental setting up, the fraction of protein that penetrated HeLa cells via CXCR4 was reduced from almost 70 % (in the parental T22-GFP-H6), to around 30 % (Figure 1 C). This fact indicated that the presence of HA2, in this precise insertion site, minimized the CXCR4 specificity of the material, probably linked to the receptor-independent fusogenic character conferred by the viral segment that enhanced, at the same time and as expected, cell penetrability. Therefore, an obvious concern was whether the extraordinary tumor targeting manifested by T22-GFP-HA2-H6 was the result of the expected CXCR4 selectivity or

11

it was rather mediated by a combination of the cell-penetrating properties of HA2 and of an enhanced permeability and retention (EPR) effect [40, 41].

To discriminate between these two possibilities, an *in vivo* competition experiment was designed in which the CXCR4 antagonist, AMD3100 [42-47], was used to block tumor accumulation of the administered protein materials. As observed (Figure 4 A, B), the antagonist dramatically minimized the occurrence of T22-GFP-H6 nanoparticles in tumoral tissues, supporting again the role of T22 in active targeting for CXCR4$^+$ cancers. Interestingly, AMD3100 equally reduced the tumor accumulation of T22-GFP-HA2-H6 nanoparticles, at levels comparable to those determined for T22-GFP-H6 (Figure 4 B). This result confirmed that T22 was fully active in T22-GFP-HA2-H6 as a targeting agent, and even a certain reduction of specificity could not be completely discarded, the tumor deposition of this construct was the result of an active targeting process. AMD3100 did not promote any important reduction in the levels of the protein in liver and kidney, supporting the background nature of the GFP emission in these non-target organs. The numerical analyses of the accumulated materials (area below the curve, Figure 4 C), was fully convincing regarding the superiority of T22-GFP-HA2-H6 as a CXCR4-targeted material, that combined the cell specificity of T22 and the cell-penetrating abilities empowered by HA2. HA2 activities were clearly dependent of the insertion site, as in T22-HA2-GFP-H6, this segment failed to enhance the properties of the protein material relevant to its intended roles as drug vehicle. Clearly, the accommodation site and molecular environment was relevant to the fusogenic properties of the whole construct.
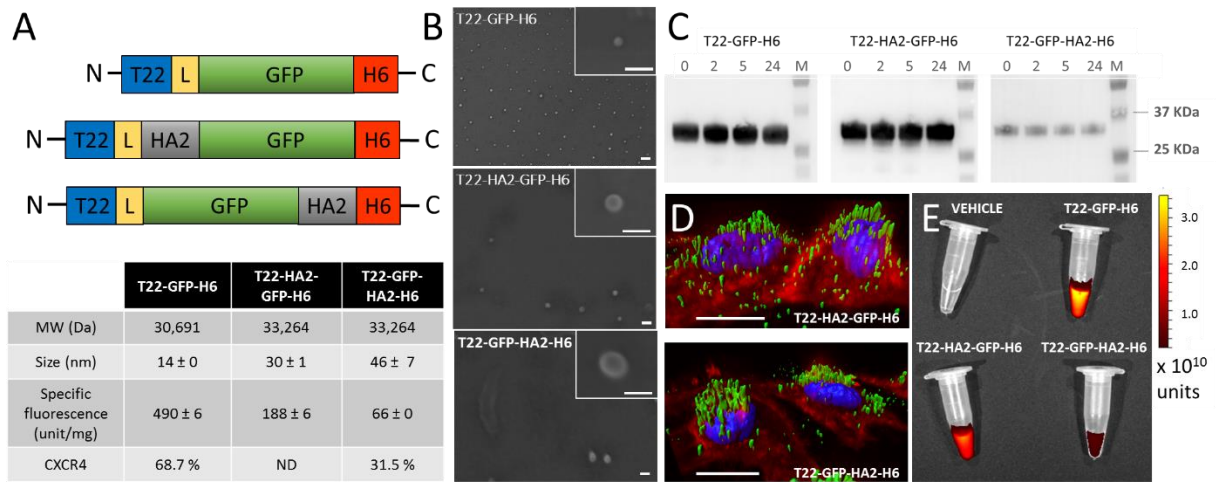

4. Conclusions

The combination of a tumor-homing peptide (T22) and a fusogenic peptide (HA2) in modular protein nanoparticles dramatically enhances the selective and efficient accumulation of the material in target tissues, proving cooperativity (rather than exclusiveness) between membrane activity and receptor-based tumor cell targeting. The specific binding to the tumoral marker CXCR4 appears to be higher in the animal models compared to the cell culture, probably due to the smaller amounts of protein that reach targeted cell per time unit. The functional recruitment in self-assembling protein nanoparticles is then seen here as a powerful approach to minimize lysosomal degradation of protein materials, a major bottleneck in the protein-based intracellular delivery of drugs and other molecules [20] in clinical or diagnostic contexts. In particular, the T22-GFP-HA2-H6 protein nano-carrier could be used to develop highly potent anticancer therapies, selectively delivered to the cytosol of CXCR4$^+$ cancer cells. This can be done by the generation of nanoconjugates that incorporate low molecular weight chemotherapeutics, unstable at lysosomal pH values [48], or protein-only nanoparticles integrating antitumor protein domains [37].

Acknowledgements

14

Figure 1. Protein materials and their respective properties. A. Schematic representation of the polypeptidic building blocks used in the study. Box sizes are only indicative. T22 is a CXCR4 specific ligand [38]. L designates the peptidic linker GGSSRSS. HA2 is the fusogenic HA2 peptide from the influenza virus hemagglutinin [27-29]. GFP is the enhanced GFP version [49]. H6 is a hexahistidine tail. Details of the aa sequences can be found elsewhere [33]. A summary of relevant properties of the nanoparticles is found in the table at the bottom. The percentage of nanoparticle entrance inhibited by the CXCR4 antagonist AMD3100 in cell culture had been previously determined [33]. B. Representative FESEM images of the assembled nanoparticles. Bars represent 40 nm. C. Stability of T22-GFP-H6, T22-HA2-GFP-H6 and T22-GFP-HA2-H6 in human serum determined by Western blot, upon incubation with human serum at 37 ºC (at 0, 2, 5 and 24 h). M indicates the molecular markers. D. Isosurface representation of cultured HeLa cells within a 3D volumetric z axes stack upon incubation with 0.5 µM protein nanoparticles for 24 h. The cell membrane was labelled with CellMask (rendering a red signal), the nuclear DNA was labelled with Hoeschst 33342 (rendering a blue signal) and protein nanoparticles are seen in green because of their intrinsic fluorescence. Bars indicate 5 µm. E. Fluorescence of the materials just before *in vivo* i.v. administration.
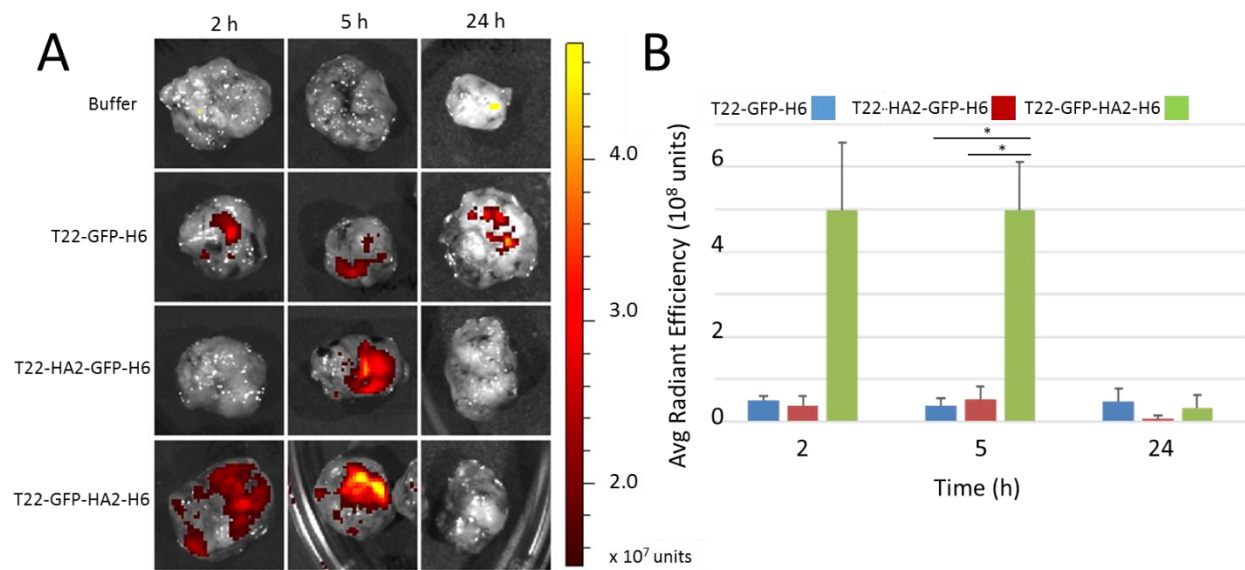
Figure 2. Tumor biodistribution of nanoparticles in a mouse model of human colorectal cancer highly expressing CXCR4. A. Representative *ex vivo* images of GFP-emitted fluorescence by the tumor at 2 h, 5 h and 24 h after the i.v. administration of 200 µg dose of each protein nanoparticle in the patient-derived M5 subcutaneous colorectal cancer model. B. Quantitative analysis of tumor emitted fluorescence by each nanoparticle at the studied time points. Data were corrected by specific fluorescence of each protein, so they are indicative of protein amounts. *, $p < 0.05$.
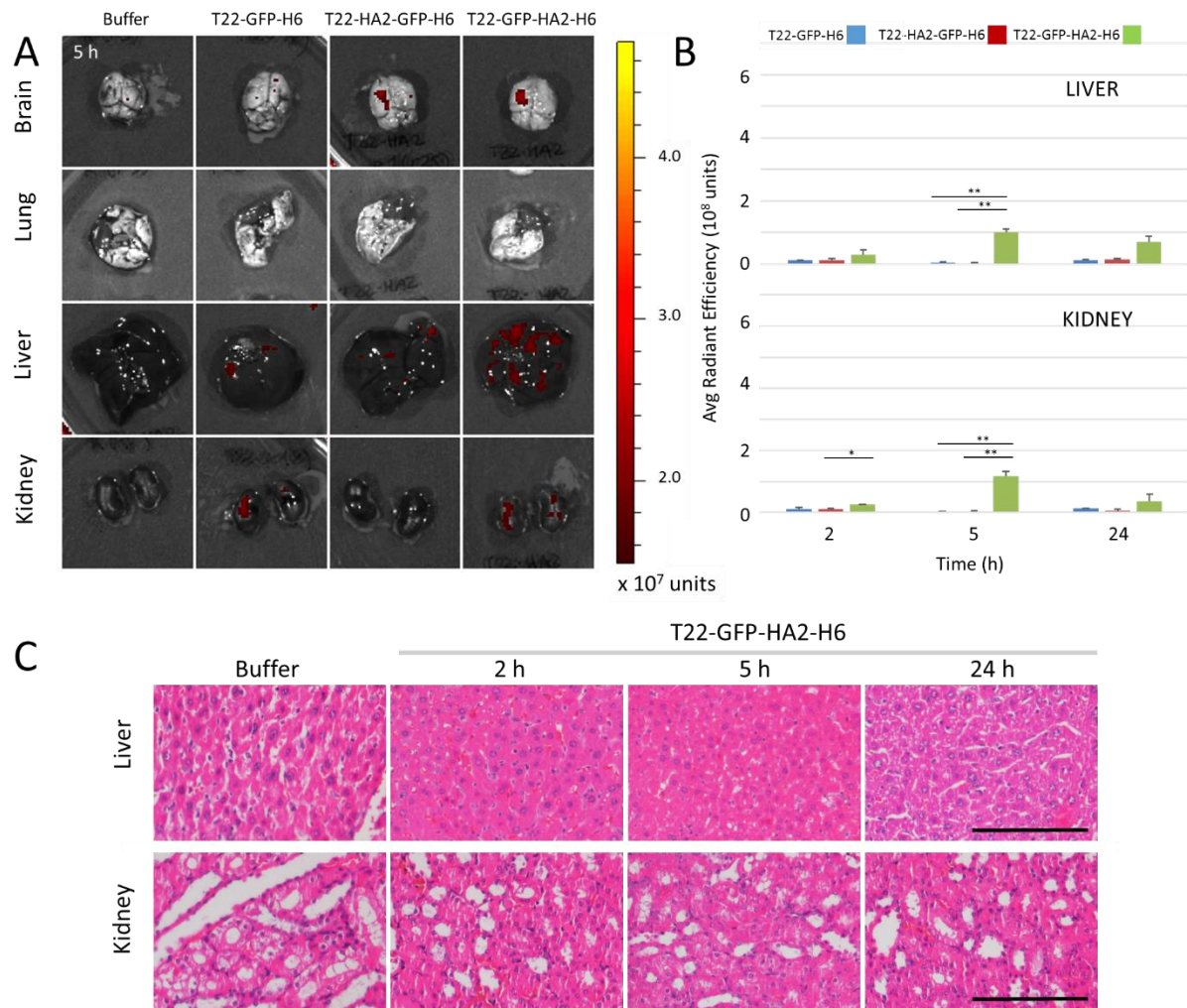
Figure 3. Biodistribution and lack of toxicity of the nanoparticles in non-target organs. A**.** Representative *ex vivo* images of GFP-emitted fluorescence in the main non-tumor organs at 2 h, 5 h and 24 h after the i.v. injection of 200 µg dose of each protein nanoparticle in the SC M5 colorectal cancer model B. Quantitative analysis of liver- and kidney- emitted fluorescence by each nanoparticle at the studied time points.. *, *p*<0.05; **, *p*<0.01. C. Absence of histopathological alterations in liver or kidney in H&E stained tissue sections, at the studied time points after the administration of the T22-GFP-HA2-H6 nanoparticle. Bars indicate 250 µm.
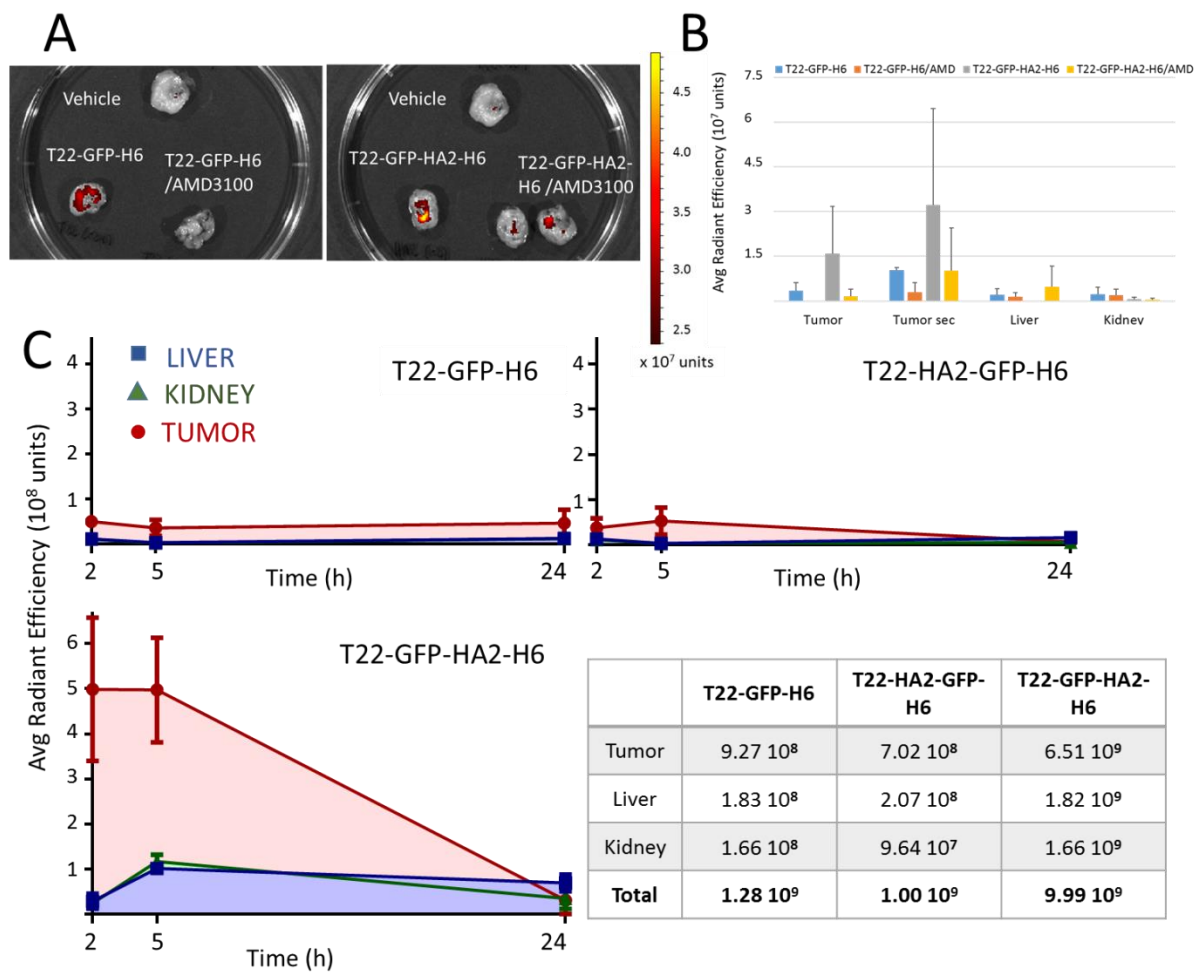
Figure 4. CXCR4-dependent biodistribution of nanoparticles and exposure in tumor and non-tumor organs. A. Inhibition of T22-GFP-H6 or T22-GFP-HA2-H6 nanoparticle accumulation in tumor tissue 5 h after their i.v. injection (200 µg dose) by the administration of the CXCR4 antagonist AMD3100 (10 mg/kg dose, 1 h before, 1 h after and 2 h after nanoparticle injection). B. Quantitation of the fluorescence-emitted in tumor (images in panel A), liver and kidney. Notice CXCR4-dependence for tumor accumulation for both nanoparticles and their lack of receptor-dependence and low level of accumulation in liver and kidney. C. Graphic representation of total nanoparticle exposure (Area under the curve: AUC = FLI emission x time (h)) registered in tumor and non-tumor organs along the studied period (2-24 h) for all three tested nanoparticles (200 µg dose) using the SC M5 colorectal cancer model, and its quantitation. Fluorescence emission intensity (FLI) signal from experimental mice was calculated subtracting the FLI auto-fluorescence of control buffer-treated mice. FLI, fluorescent intensity (expressed as average radiant efficiency).

Competing interests. RM, EV and AV are cofounders of Nanoligent SL, a company devoted to the development of anticancer drugs based on the peptide T22.

References

[1] Vazquez E, Mangues R, Villaverde A. Functional recruitment for drug delivery through protein-based nanotechnologies. Nanomedicine. 2016;11:1333-6.

[2] Loo Y, Goktas M, Tekinay AB, Guler MO, Hauser CA, Mitraki A. Self-Assembled Proteins and Peptides as Scaffolds for Tissue Regeneration. Advanced healthcare materials. 2015;4:2557-86.

[3] Sutherland T.D. Rapson T.D. HMG, Church J.S. Recombinant Structural Proteins and Their Use in Future Materials. . In: Parry D. SJ, editor. Fibrous Proteins: Structures and Mechanisms Cham: Springer; 2017.

[4] Kobayashi N, Arai R. Design and construction of self-assembling supramolecular protein complexes using artificial and fusion proteins as nanoscale building blocks. Current opinion in biotechnology. 2017;46:57-65.

[5] Yeates TO. Geometric Principles for Designing Highly Symmetric Self-Assembling Protein Nanomaterials. Annual review of biophysics. 2017;46:23-42.

[6] Schwarz B, Uchida M, Douglas T. Biomedical and Catalytic Opportunities of Virus-Like Particles in Nanotechnology. Advances in virus research. 2017;97:1-60.

[7] Sutherland TD, Huson MG, Rapson TD. Rational design of new materials using recombinant structural proteins: Current state and future challenges. Journal of structural biology. 2018;201:76-83.

[8] de Marco A, Ferrer-Miralles N, Garcia-Fruitos E, Mitraki A, Peternel S, Rinas U, Trujillo-Roldán MA, Valdez-Cruz NA, Vázquez E, Villaverde A. Bacterial inclusion bodies are industrially exploitable amyloids. FEMS microbiology reviews. 2019;43:53-72.

[9] DiMarco RL, Heilshorn SC. Multifunctional materials through modular protein engineering. Advanced materials. 2012;24:3923-40.

[10] Webber MJ, Appel EA, Meijer EW, Langer R. Supramolecular biomaterials. Nature materials. 2016;15:13-26.

[11] Duncan R, Gaspar R. Nanomedicine(s) under the microscope. Molecular pharmaceutics. 2011;8:2101-41.

[12] Lammers T, Kiessling F, Ashford M, Hennink W, Crommelin D, Storm G. Cancer nanomedicine: Is targeting our target? Nature reviews Materials. 2016;1.

[13] Lee MS, Dees EC, Wang AZ. Nanoparticle-Delivered Chemotherapy: Old Drugs in New Packages. Oncology. 2017;31:198-208.

[14] Lu L, Qi H, Zhu J, Sun WX, Zhang B, Tang CY, Cheng Q. Vascular-homing peptides for cancer therapy. Biomedicine & pharmacotherapy = Biomedecine & pharmacotherapie. 2017;92:187-95.

[15] David A. Peptide ligand-modified nanomedicines for targeting cells at the tumor microenvironment. Advanced drug delivery reviews. 2017;119:120-42.

[16] Ozturk-Atar K, Eroglu H, Calis S. Novel advances in targeted drug delivery. Journal of drug targeting. 2018;26:633-42.

[17] Alavi M, Hamidi M. Passive and active targeting in cancer therapy by liposomes and lipid nanoparticles. Drug metabolism and personalized therapy. 2019.

[18] Dey P, Rathod M, De A. Targeting stem cells in the realm of drug-resistant breast cancer. Breast cancer. 2019;11:115-35.

[19] Varkouhi AK, Scholte M, Storm G, Haisma HJ. Endosomal escape pathways for delivery of biologicals. Journal of controlled release : official journal of the Controlled Release Society. 2011;151:220-8.

[20] Shete HK, Prabhu RH, Patravale VB. Endosomal escape: a bottleneck in intracellular delivery. Journal of nanoscience and nanotechnology. 2014;14:460-74.

[21] Rueda F, Cespedes MV, Conchillo-Sole O, Sanchez-Chardi A, Seras-Franzoso J, Cubarsi R, Gallardo A, Pesarrodona M, Ferrer-Miralles N, Daura X, Vázquez E, García-Fruitós E, Mangues R, Unzueta U, Villaverde A. Bottom-Up Instructive Quality Control in the Biofabrication of Smart Protein Materials. Advanced materials. 2015;27:7816-22.

[22] Zhang SS, Han ZP, Jing YY, Tao SF, Li TJ, Wang H, Wang Y, Li R, Yang Y, Zhao X, Xu XD, Yu ED, Rui YC, Liu HJ, Zhang L, Wei LX. CD133(+)CXCR4(+) colon cancer cells exhibit metastatic potential and predict poor prognosis of patients. BMC medicine. 2012;10:85.

[23] Wang Y, Xie Y, Oupicky D. Potential of CXCR4/CXCL12 Chemokine Axis in Cancer Drug Delivery. Current pharmacology reports. 2016;2:1-10.

[24] Sanchez JM, Sanchez-Garcia L, Pesarrodona M, Serna N, Sanchez-Chardi A, Unzueta U, Mangues R, Vázquez E, Villaverde A. Conformational Conversion during Controlled Oligomerization into Nonamylogenic Protein Nanoparticles. Biomacromolecules. 2018;19:3788-97.

[25] Lopez-Laguna H, Unzueta U, Conchillo-Sole O, Sanchez-Chardi A, Pesarrodona M, Cano-Garrido O, Voltà E, Sánchez-García L, Serna N, Saccardo P, Mangues R, Villaverde A, Vázquez E. Assembly of histidine-rich protein materials controlled through divalent cations. Acta biomaterialia. 2019;83:257-64.

[26] Cespedes MV, Unzueta U, Avino A, Gallardo A, Alamo P, Sala R, Sánchez-Chardi A, Casanova I, Mangues MA, Lopez-Pousa A, Eritja R, Villaverde A, Vázquez E, Mangues R. Selective depletion of metastatic stem cells as therapy for human colorectal cancer. EMBO molecular medicine. 2018. e8772.

[27] Wagner E, Plank C, Zatloukal K, Cotten M, Birnstiel ML. Influenza virus hemagglutinin HA-2 N-terminal fusogenic peptides augment gene transfer by transferrin-polylysine-DNA complexes: toward a synthetic virus-like gene-transfer vehicle. Proceedings of the National Academy of Sciences of the United States of America. 1992;89:7934-8.

[28] Skehel JJ, Cross K, Steinhauer D, Wiley DC. Influenza fusion peptides. Biochemical Society transactions. 2001;29:623-6.

[29] Neundorf I, Rennert R, Hoyer J, Schramm F, Lobner K, Kitanovic I, Wölfl S. Fusion of a Short HA2-Derived Peptide Sequence to Cell-Penetrating Peptides Improves Cytosolic Uptake, but Enhances Cytotoxic Activity. Pharmaceuticals. 2009;2:49-65.

[30] Chen YL, Li JH, Yu CY, Lin CJ, Chiu PH, Chen PW, Lin CC, Chen WJ. Novel cationic antimicrobial peptide GW-H1 induced caspase-dependent apoptosis of hepatocellular carcinoma cell lines. Peptides. 2012;36:257-65.

[31] Kim S, Kim D, Jung HH, Lee IH, Kim JI, Suh JY, Jon S. Bio-inspired design and potential biomedical applications of a novel class of high-affinity peptides. Angewandte Chemie. 2012;51:1890-4.

[32] Lonn P, Kacsinta AD, Cui XS, Hamil AS, Kaulich M, Gogoi K, Dowdy SF. Enhancing Endosomal Escape for Intracellular Delivery of Macromolecular Biologic Therapeutics. Scientific reports. 2016;6:32301.

[33] Sanchez-Garcia L, Serna N, Mattanovich M, Cazzanelli P, Sanchez-Chardi A, Conchillo-Sole O, Cortés F, Daura X, Unzueta U, Mangues R, Villaverde A, Vázquez E. The fusogenic peptide HA2 impairs selectivity of CXCR4-targeted protein nanoparticles. Chemical communications. 2017;53:4565-8.

[34] Serna N, Sanchez JM, Unzueta U, Sanchez-Garcia L, Sanchez-Chardi A, Mangues R, Vázquez E, Villaverde A. Recruiting potent membrane penetrability in tumor cell-targeted protein-only nanoparticles. Nanotechnology. 2019;30:115101.

[35] Cespedes MV, Unzueta U, Tatkiewicz W, Sanchez-Chardi A, Conchillo-Sole O, Alamo P, Xu Z, Casanova I, Corchero JL, Pesarrodona M, Cedano J, Daura X, Ratera I, Veciana J, Ferrer-Miralles N, Vazquez E, Villaverde A, Mangues R. In vivo architectonic stability of fully de novo designed protein-only nanoparticles. ACS nano. 2014;8:4166-76.

[36] Falgas A, Pallares V, Unzueta U, Cespedes MV, Arroyo-Solera I, Moreno MJ, Gallardo A, Mangues MA, Sierra J, Villaverde A, Vázquez E, Mangues R, Casanova I. A CXCR4-targeted nanocarrier achieves highly selective tumor uptake in diffuse large B-cell lymphoma mouse models. Haematologica. 2019. doi: 10.3324/haematol.2018.211490.

[37] Sanchez-Garcia L, Serna N, Alamo P, Sala R, Cespedes MV, Roldan M, Sánchez-Chardi A, Unzueta U, Casanova I, Mangues R, Vázquez E, Villaverde A. Self-assembling toxin-based nanoparticles as self-delivered antitumoral drugs. Journal of controlled release. 2018; 274:81-92

[38] Tamamura H, Imai M, Ishihara T, Masuda M, Funakoshi H, Oyake H, Murakami T, Arakaki R, Nakashima H, Otaka A, Ibuka T, Waki M, Matsumoto A, Yamamoto N, Fujii N. Pharmacophore identification of a chemokine receptor (CXCR4) antagonist, T22 ([Tyr(5,12),Lys7]-polyphemusin II), which specifically blocks T cell-line-tropic HIV-1 infection. Bioorganic & medicinal chemistry. 1998;6:1033-41.

[39] **Unzueta U, Céspedes MV, Ferrer-Miralles N, Casanova I, Cedano J, Corchero JL, Domingo-Espín J, Villaverde A, Mangues R, Vázquez E.Intracellular CXCR4^{+} cell targeting with T22-empowered protein-only nanoparticles. Int J Nanomedicine. 2012;7:4533-44.** [40] Nel A, Ruoslahti E, Meng H. New Insights into "Permeability" as in the Enhanced Permeability and Retention Effect of Cancer Nanotherapeutics. ACS nano. 2017;11:9567-9.

[41] Kalyane D, Raval N, Maheshwari R, Tambe V, Kalia K, Tekade RK. Employment of enhanced permeability and retention effect (EPR): Nanoparticle-based precision tools for targeting of therapeutic and diagnostic agent in cancer. Materials science & engineering C, Materials for biological applications. 2019;98:1252-76.

[42] Ahmad N, Masood AK, Owais M. Fusogenic potential of prokaryotic membrane lipids. Implication in vaccine development. European journal of biochemistry. 2001;268:5667-75.

[43] Song JS, Kang CM, Kang HH, Yoon HK, Kim YK, Kim KH, Moon HS, Park SH. Inhibitory effect of CXC chemokine receptor 4 antagonist AMD3100 on bleomycin induced murine pulmonary fibrosis. Experimental & molecular medicine. 2010;42:465-72.

[44] Yu M, Gang EJ, Parameswaran R, Stoddart S, Fei F, Schmidhuber S, Park E, Hsieh YT, Yang AS, Groffen J, Heisterkamp N, Kim YM. AMD3100 sensitizes acute lymphoblastic leukemia cells to chemotherapy in vivo. Blood cancer journal. 2011;1:e14.

[45] Im JY, Min WK, Park MH, Kim N, Lee JK, Jin HK, Choi JY, Kim SY, Bae JS. AMD3100 improves ovariectomy-induced osteoporosis in mice by facilitating mobilization of hematopoietic stem/progenitor cells. BMB reports. 2014;47:439-44.

[46] Poty S, Desogere P, Goze C, Boschetti F, D'Huys T, Schols D, Cawthorne C, Archibald SJ, Maëcke HR, Denat F. New AMD3100 derivatives for CXCR4 chemokine receptor targeted molecular imaging studies: synthesis, anti-HIV-1 evaluation and binding affinities. Dalton transactions. 2015;44:5004-16.

[47] Jung YH, Lee DY, Cha W, Kim BH, Sung MW, Kim KH, Ahn SH.Antitumor effect of CXCR4 antagonist AMD3100 on the tumorigenic cell line of BHP10-3 papillary thyroid cancer cells. Head & neck. 2016;38:1479-86.

[48] Rawat A, Vaidya B, Khatri K, Goyal AK, Gupta PN, Mahor S, Paliwal R, Rai S, Vyas SP. Targeted intracellular delivery of therapeutics: an overview. Die Pharmazie. 2007;62:643-58.

[49] Cinelli RA, Ferrari A, Pellegrini V, Tyagi M, Giacca M, Beltram F. The enhanced green fluorescent protein as a tool for the analysis of protein dynamics and localization: local fluorescence study at the single-molecule level. Photochemistry and photobiology. 2000;71:771-6.